Vortex- and convective-scale structure and evolution during the rapid intensification of Hurricane Earl (2010)

Robert Rogers[1], Paul Reasor[1], Sylvie Lorsolo[2], Jun Zhang[2]

[1]NOAA/AOML Hurricane Research Division
[2]University of Miami/CIMAS

MOTIVATION

One of the most challenging and important aspects of tropical cyclone dynamics is rapid intensification (RI). Recent work has examined smaller-scale characteristics of TC's undergoing RI, including symmetric and asymmetric processes (Montgomery and Smith 2011), convective bursts and vortical hot towers (VHT's; Nguyen et al. 2008, Reasor et al. 2009, Guimond et al. 2010) and the broader spectrum of updrafts (Rogers 2010). What has not been possible is a detailed documentation of the evolution of the inner core of a TC undergoing RI, including observations of both vortex- and convective-scale structures. Such a documentation is important to test hypotheses of RI dealing with issues such as the relative importance of environmental vs. inner-core processes in RI, symmetric vs. asymmetric processes during RI, the role of bursts and VHT's, and inner-core humidifcation.

STORM SUMMARY AND DATA

Summary and aircraft coverage

Hurricane Earl was the fifth tropical cyclone of the 2010 Atlantic hurricane season. Earl developed from a vigorous tropical wave in the eastern Atlantic. By the time it reached the western Atlantic near Barbados on August 28, Earl was already a tropical storm. Earl rapidly intensified as it moved west-northwest, north of the Windward Islands. NOAA, NASA, and Air Force aircraft sampled the system prior to, during, and at the end of the rapid intensification period, with less than 12 h between sampling times for the inner core and less than 24 h for the environment. This represents one of the most intensively-sampled lifecycles of rapid intensification. A preliminary analysis of the inner-core structure and evolution of Earl during its RI is presented here.
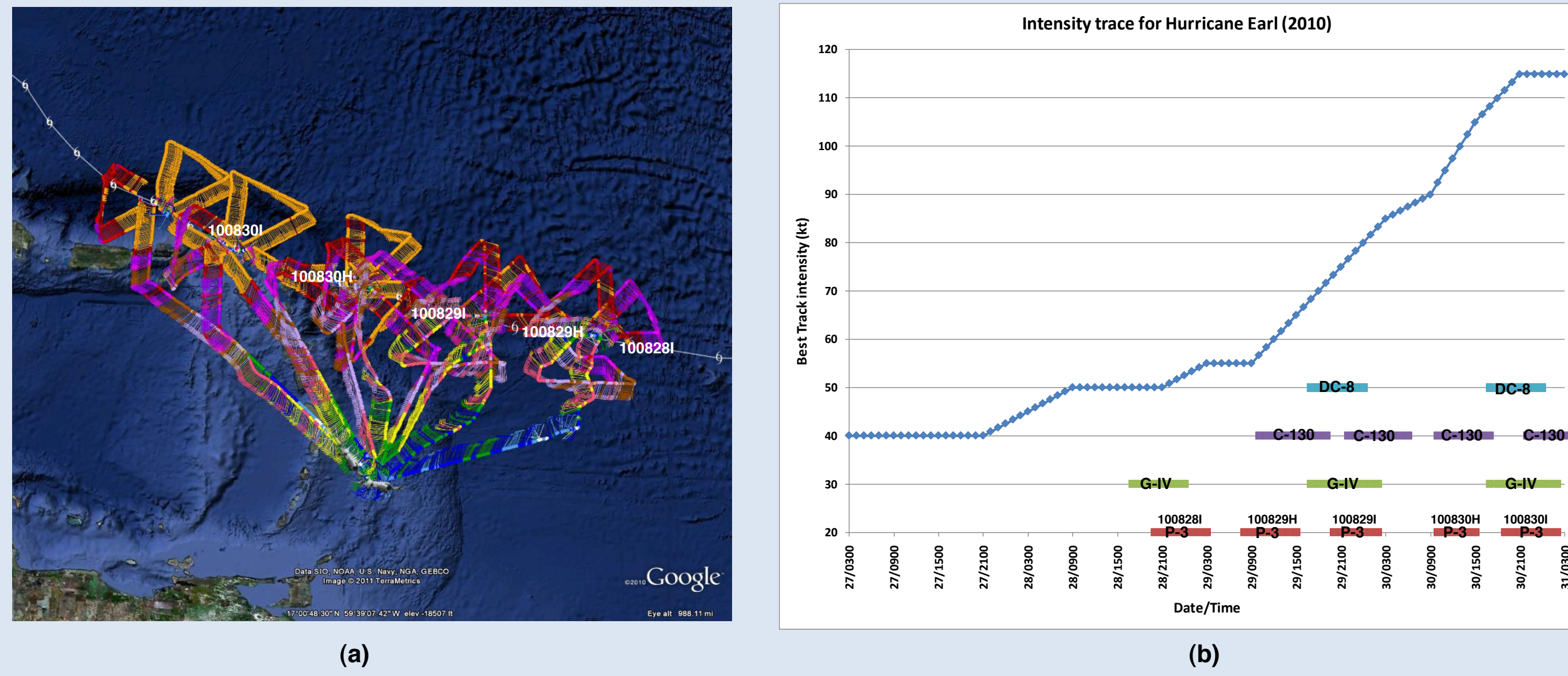

Figure 1. (a) Track and P-3 coverage of Hurricane Earl (2010). (b) Best track intensity and aircraft coverage of Earl. Flight names for P-3 missions are indicated. RI begins at 12 UTC 29 August, during the second P-3 flight (100829H).
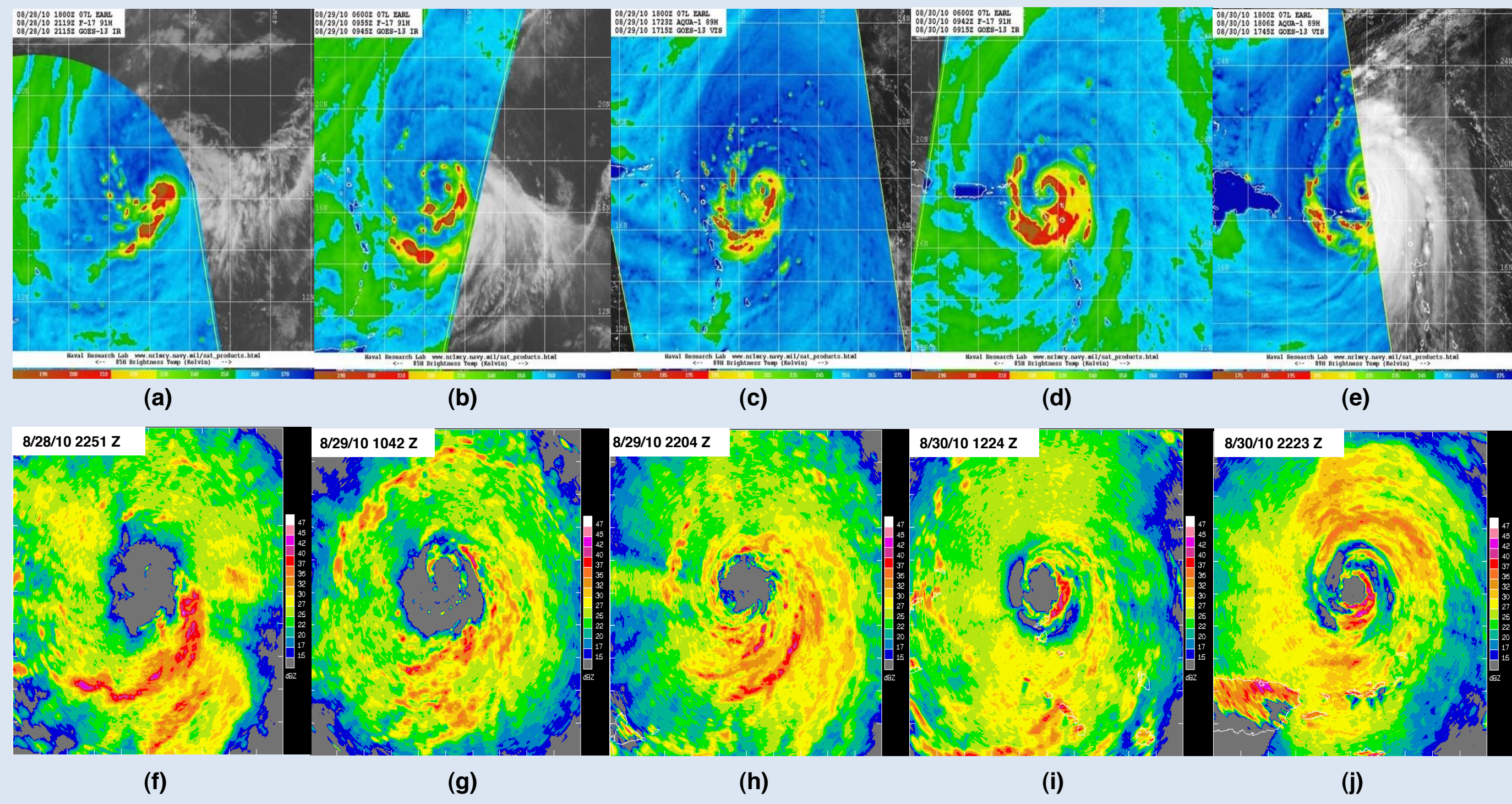
Satellite and radar depiction

Figure 2. 89-91 GHz brightness temperature (shaded, K) for Hurricane Earl (2010) at (a) 2119 UTC August 28; (b) 0955 UTC August 29; (c) 1723 UTC August 29; (d) 0942 UTC August 30; and (e) 1806 UTC August 30. NOAA P-3 lower fuselage radar images (shaded, dBZ, scale showed on right-hand side of figure) for (f) 2251 UTC 28 August; (g) 1042 UTC 29 August; (h) 2204 UTC 29 August; (i) 1224 UTC 30 August; (j) 2223 UTC 30 August. Domain size for radar images is 360 km on a side.

Data coverage

Data for this analysis comes primarily from airborne Doppler radar on the NOAA P-3 and GPS dropsondes from NOAA P-3, NASA DC-8, and Air Force C-130.
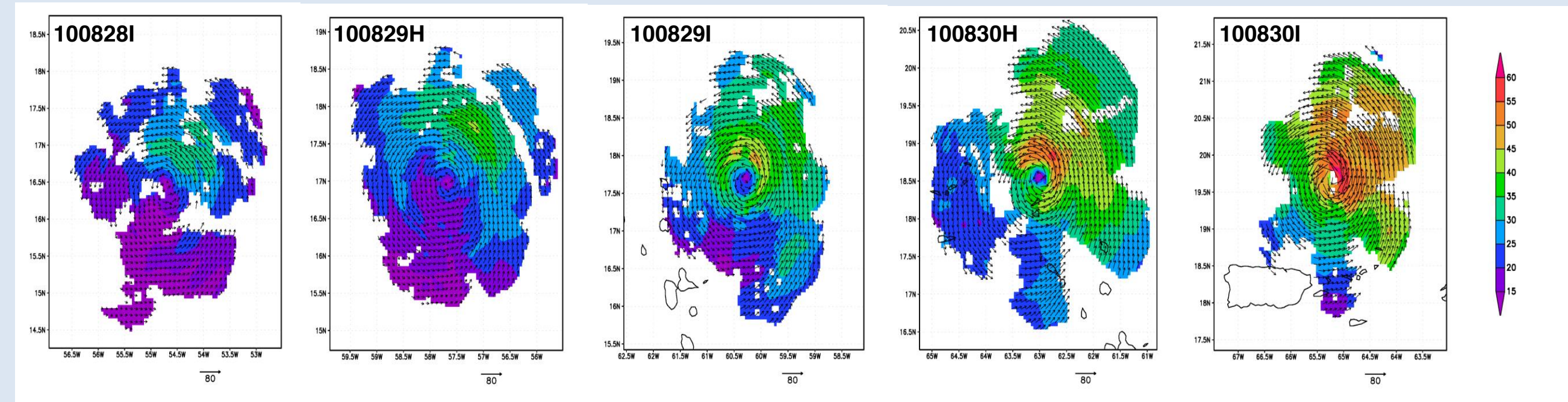

Figure 3. Composite of airborne Doppler-derived wind speeds (shaded, m s^{-1}) at 2 km altitude centered at approximately (a) 00 UTC 29 August; (b) 12 UTC 29 August; (c) 00 UTC 30 August; (d) 12 UTC 30 August; and (e) 00 UTC 31 August.
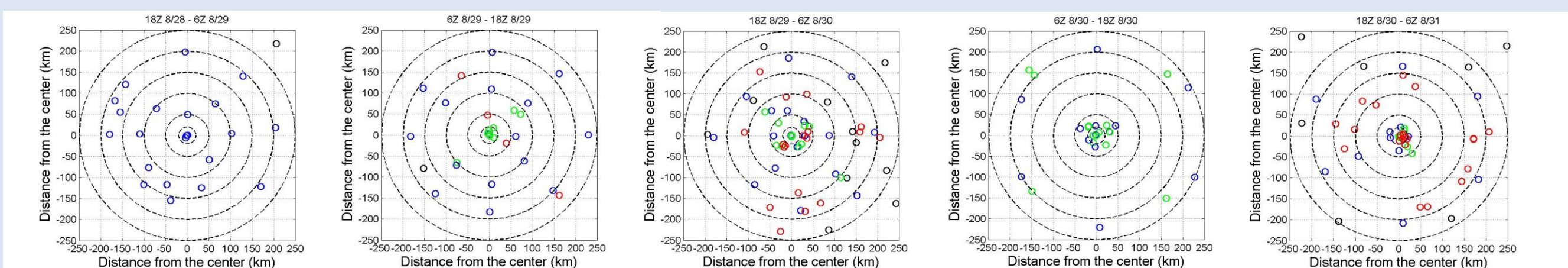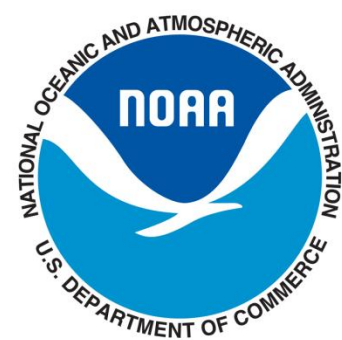
Figure 4. Location of GPS dropsondes within 250 km radius from all aircraft in a 12-h window centered at (a) 00 UTC 29 August; (b) 12 UTC 29 August; (c) 00 UTC 30 August; (d) 12 UTC 30 August; and (e) 00 UTC 31 August. Color coding for aircraft is as follows: Blue, P-3; Red, DC-8; Green, C-130.

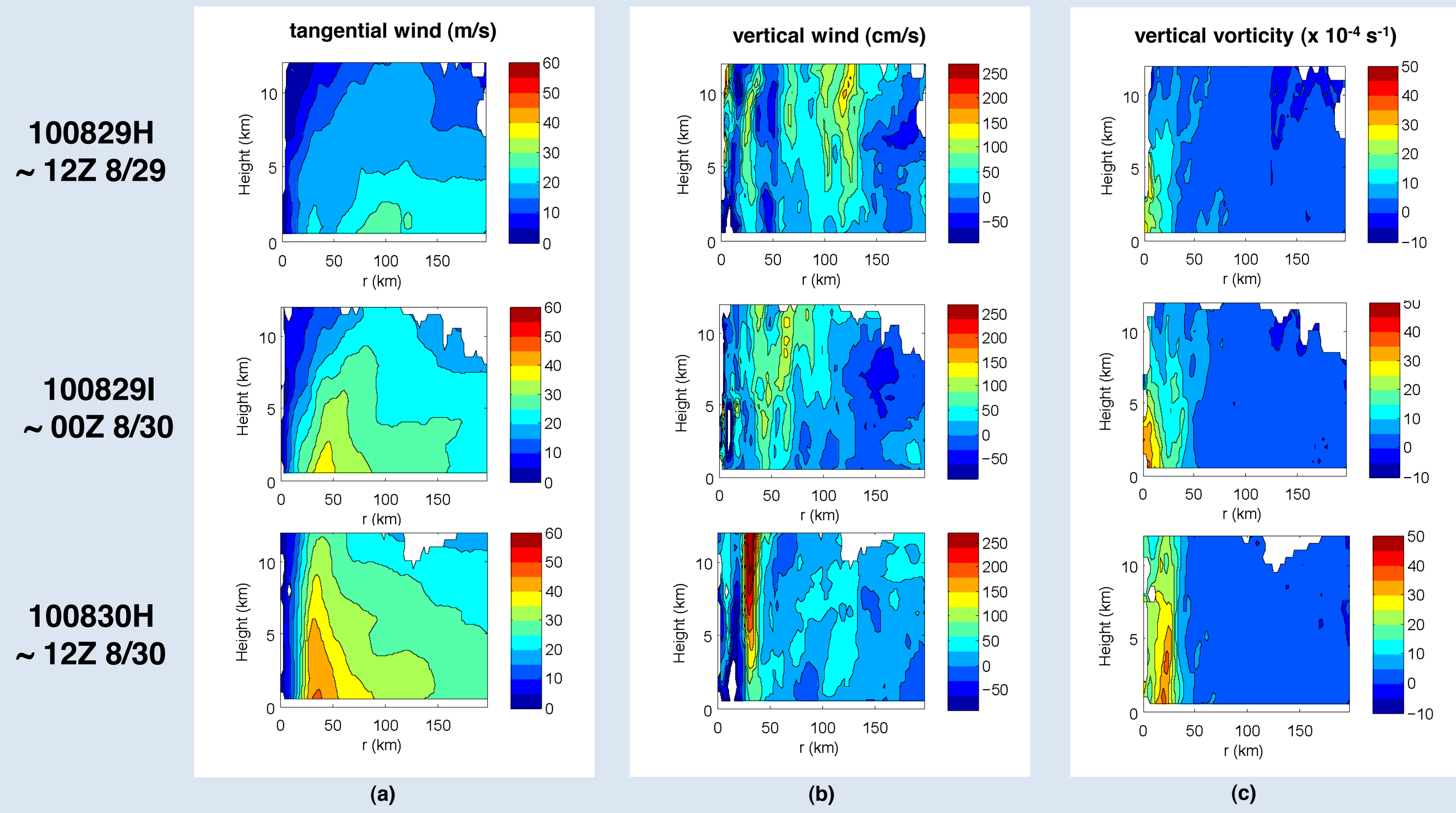## RESULTS

Symmetric vortex-scale structure and evolution

Figure 5. Radius-height plots of (a) axisymmetric tangential wind (shaded, m s^{-1}); (b) axisymmetric vertical velocity (shaded, cm s^{-1}); (c) axisymmetric vertical vorticity (shaded, x 10^{-4} s^{-1}). Top row in all figures is for Flight 100829H (approx. centered on 12 UTC 29 August), middle row is for Flight 100830I (centered on 00 UTC 30 August), bottom row is for Flight 100830H (centered on 12 UTC 30 August).

- Radius of maximum symmetric tangential wind contracts from 100 km to 35 km in 24 h (12Z 8/29 – 12Z 8/30)
- Vortex grows in depth from 5 km to > 12 km during this time
- Peak symmetric updraft contracts in radial extent and amplifies to > 2.5 m s-1
- Symmetric vorticity begins as a monopole, intensifies from 12Z 8/29 to 00Z 8/30
- Vorticity acquires a ring-like structure by 12Z 8/30 as eyewall becomes well-defined
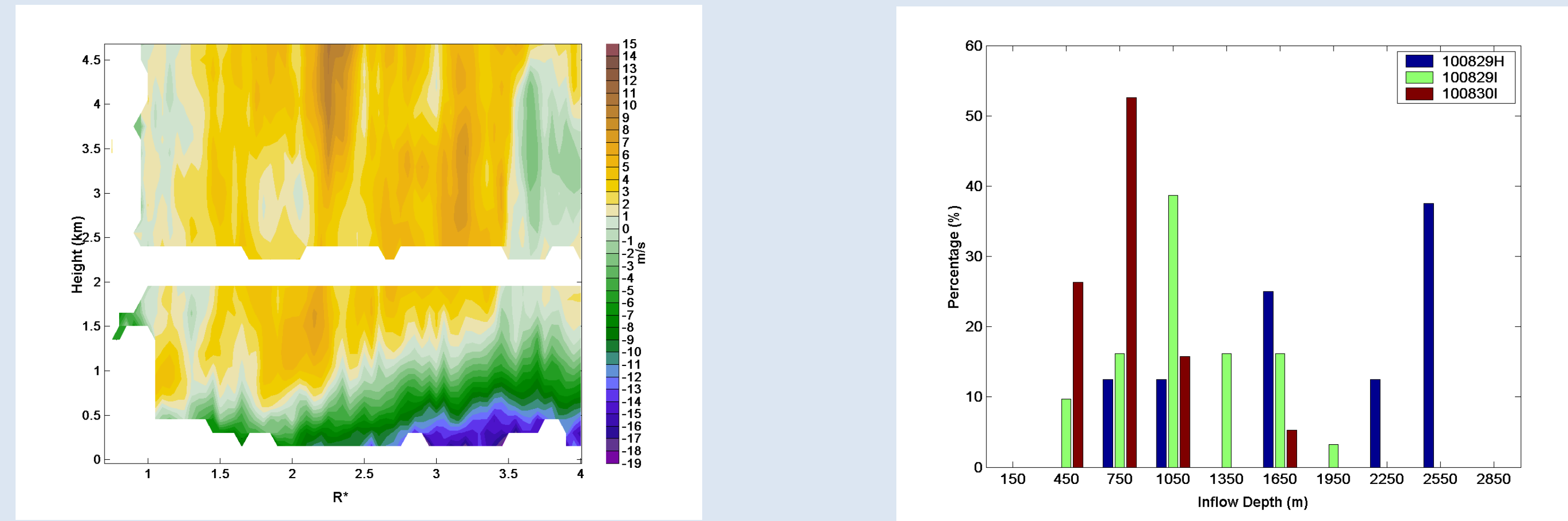
PBL inflow depth evolution

Figure 6. Doppler-derived profile of radial wind (shaded, m s^{-1}) plotted from 0.7 to 4 x radius of maximum wind (RMW) at 2334 UTC 30 August for 100830I.

Figure 7. Histogram of inflow-layer depth (%) for all radar passes between 1 and 1.5 x RMW, at intervals of 0.05, for 100829H, 100829I, 100830I.

- Radar profiles can effectively capture detailed structures of boundary layer in TCs, such as the depth of the inflow layer, especially in well-developed TCs (Lorsolo et al. 2010, Rogers et al. 2011)
- Distribution of inflow depth just outside the RMW is highly variable when system is a tropical storm, ranging from 0.75 to 2.5 km depth
- As RI proceeds and system becomes a strong hurricane, distribution of inflow depth becomes much narrower and the values shallower, ranging from 0.45 to 1 km depth.

Mean thermodynamic evolution

- Strong vertical gradient of inner-core low-level theta-e prior to onset of RI
- Significant increase in theta-e below 2.5 km as RI begins
- RH below 1 km ~90% before RI, increases to > 95% during RI
- Significant drying above 2 km as eye develops
- Deep-layer theta-e increases 10 K over entire profile during RI
- Humidity > 90% up to 6 km at beginning of RI, dries significantly at end of RI as eye develops
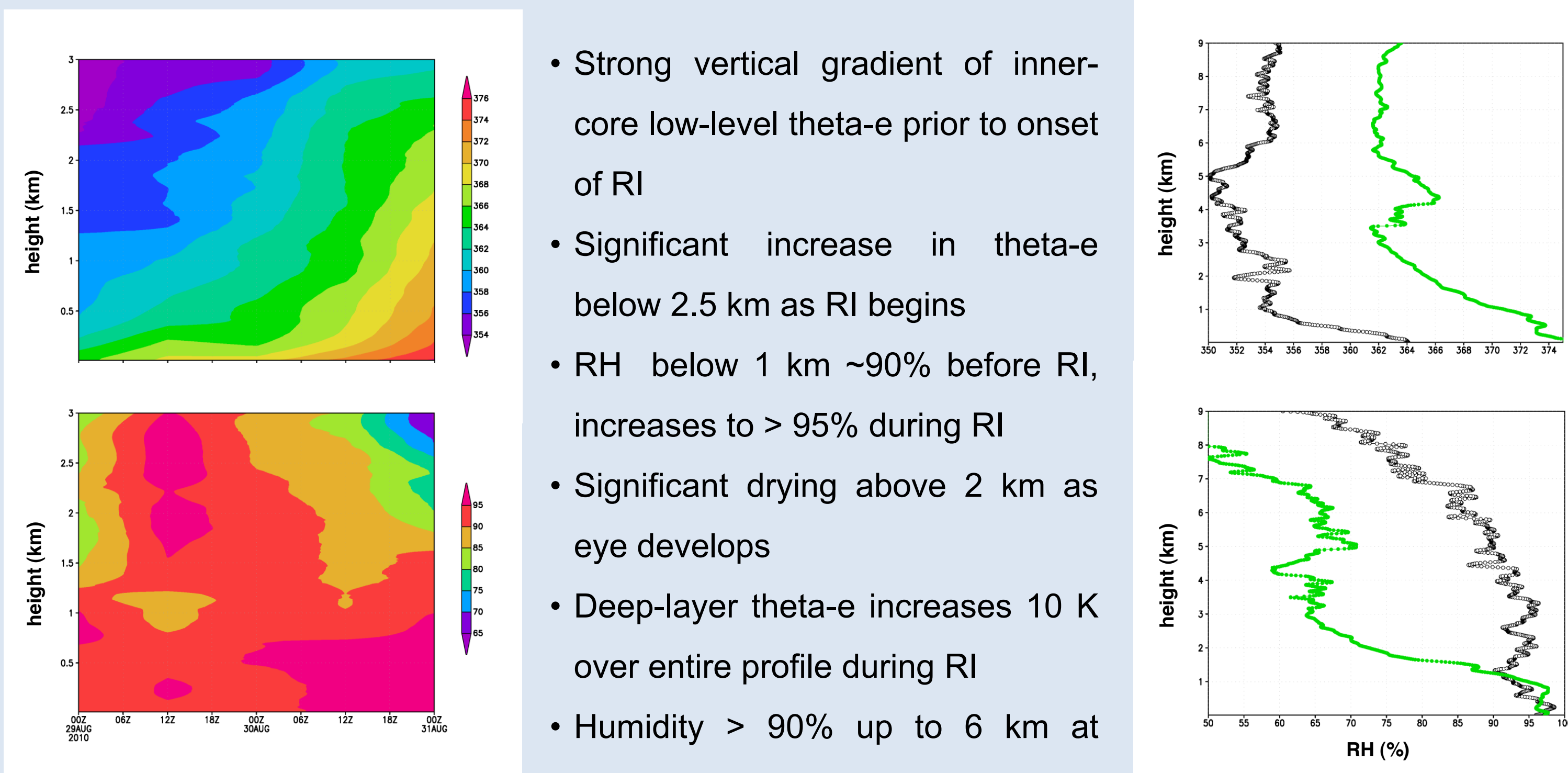- Change in RH occurs above 1 km

Figure 8. Time-height series of (a) equivalent potential temperature (shaded, K) and (b) relative humidity (shaded, %) for all dropsondes within 50 km of storm center from 00 UTC 29 August to 00 UTC 31 August.

Figure 9. Vertical profile of mean (a) equivalent potential temperature (K) and (b) relative humidity (%) for 00 UTC 30 August (black) and 00 UTC 31 August (green) for all dropsondes within 50 km of storm center.

RESULTS
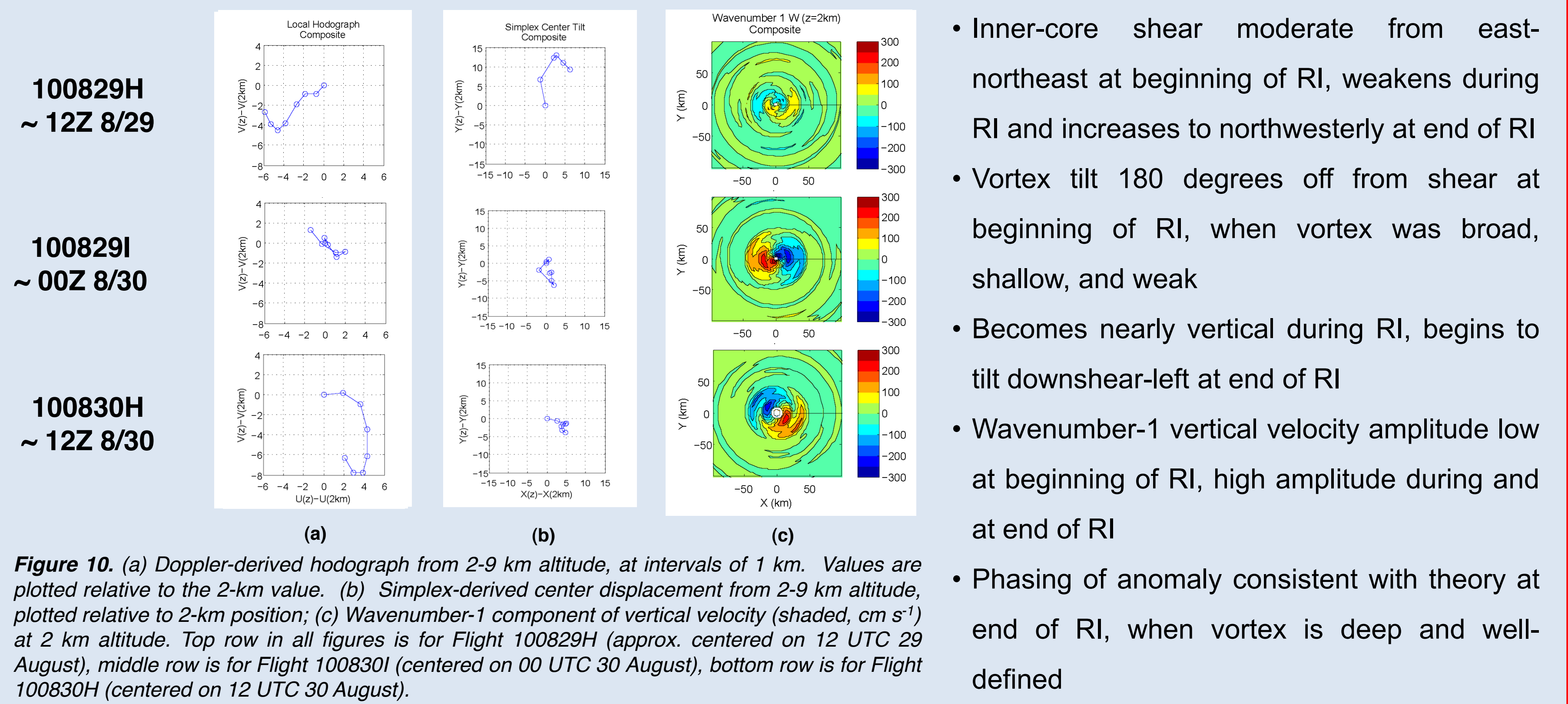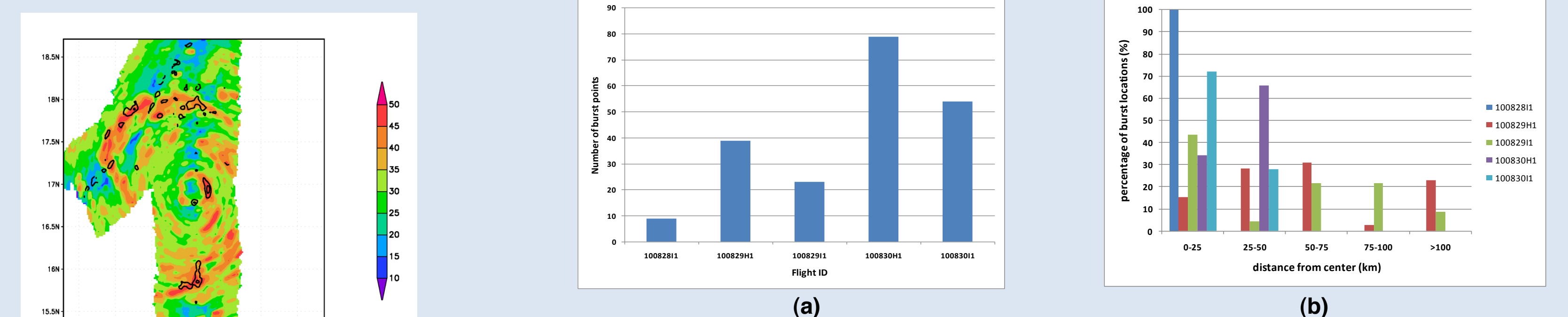
Asymmetric vortex-scale structure and evolution

Figure 10. (a) Doppler-derived hodograph from 2-9 km altitude, at intervals of 1 km. Values are plotted relative to the 2-km value. (b) Simplex-derived center displacement from 2-9 km altitude, plotted relative to 2-km position; (c) Wavenumber-1 component of vertical velocity (shaded, cm s^{-1}) at 2 km altitude. Top row in all figures is for Flight 100829H (approx. centered on 12 UTC 29 August), middle row is for Flight 100830I (centered on 00 UTC 30 August), bottom row is for Flight 100830H (centered on 12 UTC 30 August).

- Inner-core shear moderate from east-northeast at beginning of RI, weakens during RI and increases to northwesterly at end of RI
- Vortex tilt 180 degrees off from shear at beginning of RI, when vortex was broad, shallow, and weak
- Becomes nearly vertical during RI, begins to tilt downshear-left at end of RI
- Wavenumber-1 vertical velocity amplitude low at beginning of RI, high amplitude during and at end of RI
- Phasing of anomaly consistent with theory at end of RI, when vortex is deep and well-defined

Convective burst census

Convective burst defined as those locations within Doppler analysis where vertical velocity averaged over 2-6 km depth > 4 m s^{-1}, while also coincident with 2-km reflectivity > 30 dBZ, similar to Reasor et al. (2009).

Figure 11. Plot of reflectivity (shaded, dBZ) at 2 km altitude and 2-6 km averaged vertical velocity (thick contours, only 2 and 4 m s^{-1} shown) for radar pass centered at 0939 UTC 29 August during 100829H. Bursts are where vertical velocity > 4 m s^{-1} and reflectivity > 30 dBZ.

Figure 12. (a) Number of grid points flagged as a convective burst for each P-3 flight; (b) Distribution of distances of each flagged grid point from the grid center (roughly the storm center) for each flight.

- Number of burst locations increases significantly from first to second flight (marking beginning of RI), but most burst locations appear after RI has already begun
- Broad distribution of burst distances from center early in RI period, by end of RI all bursts < 50 km from center
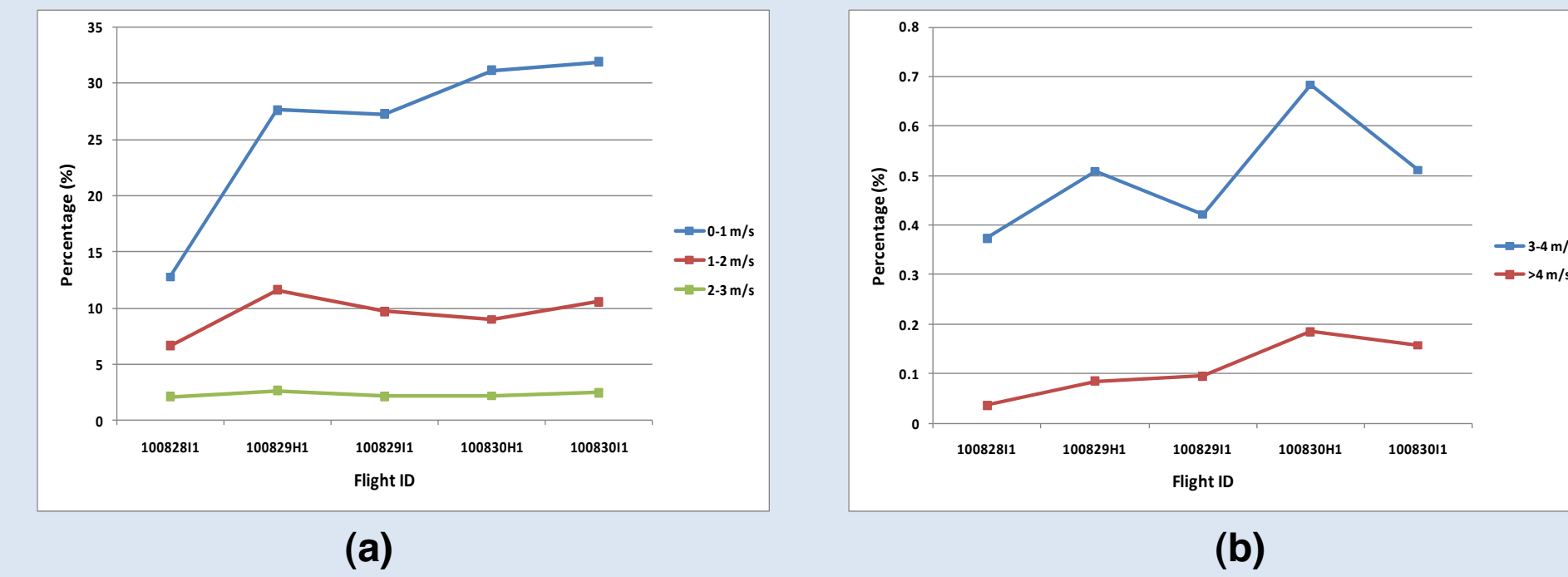
Updraft coverage

Figure 13. (a) Fractional coverage of 2-6 km updrafts between 0 and 1 m s^{-1} (blue), 1 and 2 m s^{-1} (red), and 2 and 3 m s^{-1} (green) for each P-3 flight; (b) As in (a), but for updrafts between 3 and 4 m s^{-1} (blue), and > 4 m s^{-1} (red).

- Weak to moderate updrafts (0-2 m s^{-1}) show most significant increase in fractional coverage at the beginning of RI, coverage of these drafts remains stable during RI
- Strong updrafts increase some at RI beginning, but comprise a very small percentage (< 0.5%) of area
- Largest increase in coverage of strong drafts near end of RI
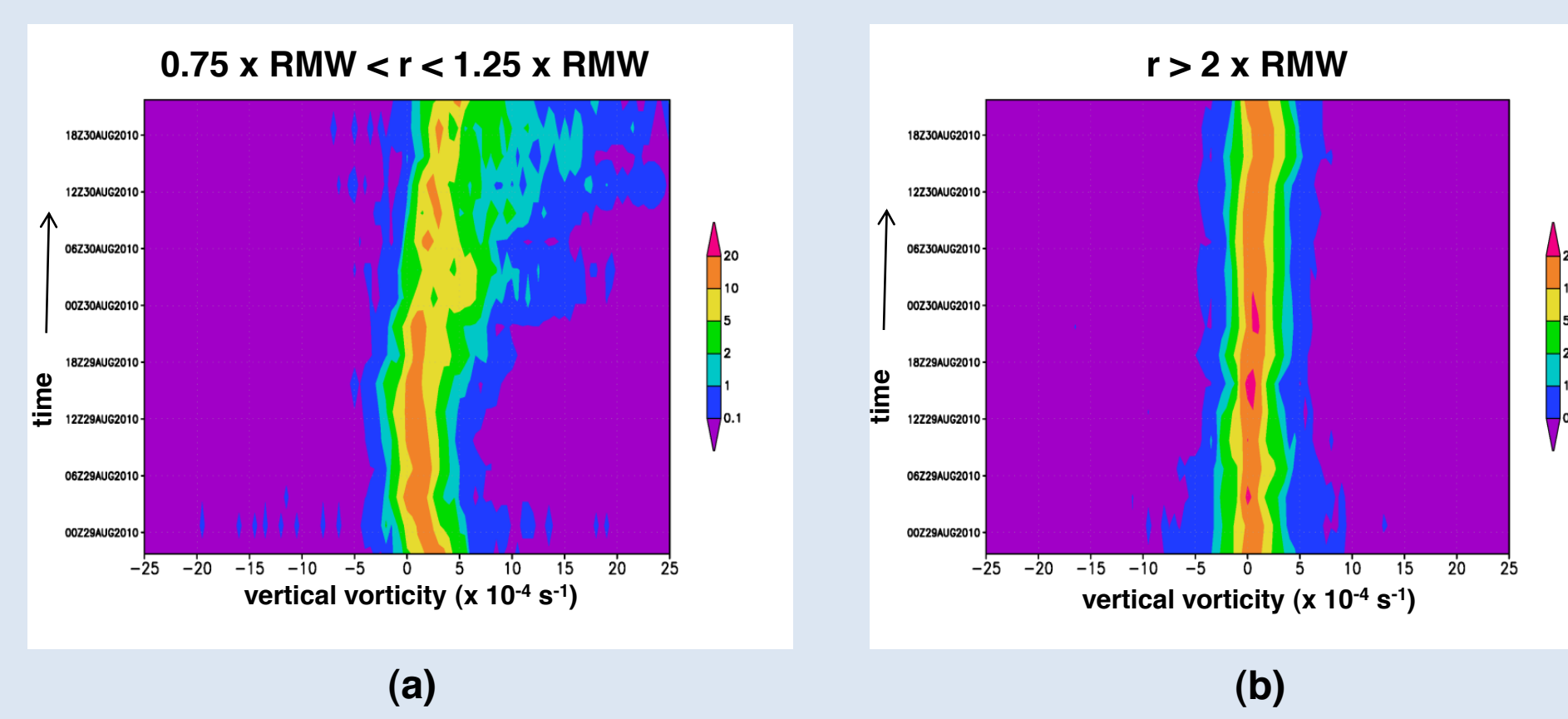
Evolution of vorticity distribution

Figure 14. Time evolution of probability distribution function of vertical vorticity at 3 km altitude for each radar pass during all five P-3 flights. (a) Vorticity between 0.75 and 1.25 x RMW; (b) Vorticity outside 2 x RMW. (NOTE: Actual distribution of data is non-uniform in time. Within each flight each radar pass separated by about 1-1.5 h, with about 8 h between flights.)

- Modal value of eyewall vorticity doubles during RI
- Vorticity distribution in eyewall symmetric at beginning of RI, becomes positively skewed during RI
- Maximum increase in skewness coincident with maximum increase in coverage of strongest vertical velocity cores in Fig. 13
- Outer-core vorticity distribution remains symmetric throughout RI, small increase in modal value

FUTURE WORK

- Examine additional aspects of symmetric structure and evolution, e.g., angular momentum fields and supergradient flow
- Examine additional aspects of asymmetric structure and evolution, including low-wavenumber kinematic and thermodynamic structures and high-wavenumber features such as convective bursts
- Determine additional characteristics of burst distribution such as location relative to vertical shear, location relative to local RMW
- Examine full spectrum of updrafts, vertical mass flux evolution during RI
- Calculate relationships between vertical velocity, vertical vorticity (e.g., joint PDFs)
- Identify additional features of boundary layer such as inflow magnitude and temperature and moisture fields
- Include analyses of large-scale parameters
- Add additional data sources to analysis, e.g., flight-level, SFMR fields
- Perform high-resolution (1-3 km grid length) simulations of Earl to provide better temporal coverage prior to and during RI